01 Aug 2020

A Comparison Study Using Particle Swarm Optimization Inversion Algorithm For Gravity Anomaly Interpretation Due To A 2D Vertical Fault Structure

Neil Lennart Anderson
Missouri University of Science and Technology, nanders@mst.edu

Khalid S. Essa

Mahmoud Elhussein

Recommended Citation

N. L. Anderson et al., "A Comparison Study Using Particle Swarm Optimization Inversion Algorithm For Gravity Anomaly Interpretation Due To A 2D Vertical Fault Structure," *Journal of Applied Geophysics*, vol. 179, article no. 104120, Elsevier, Aug 2020.
The definitive version is available at https://doi.org/10.1016/j.jappgeo.2020.104120

Journal of Applied Geophysics 179 (2020) 104120

Contents lists available at ScienceDirect

Journal of Applied Geophysics

journal homepage: www.elsevier.com/locate/jappgeo

A comparison study using particle swarm optimization inversion algorithm for gravity anomaly interpretation due to a 2D vertical fault structure

N.L. Anderson [a], Khalid S. Essa [b], Mahmoud Elhussein [b,*]

[a] Geosciences and Geological and Petroleum Engineering Department, Missouri University of Science and Technology, United States of America
[b] Geophysics Department, Faculty of Science, Cairo University, Giza P.O. 12613, Egypt

ARTICLE INFO

Article history:
Received 31 July 2019
Received in revised form 3 May 2020
Accepted 14 June 2020
Available online 16 June 2020

Keywords:
2D vertical fault
PSO
FHG
Depth
RMSE

ABSTRACT

A new approach to the inversion of gravity data utilizing the Particle Swarm Optimization (PSO) algorithm is used to model 2D vertical faults. The PSO algorithm is stochastic in nature; its development was motivated by the communal in-flight performance of birds looking for food. The birds are represented by particles (or models). Individual particles have a location and a velocity vector. The location vectors represent the parameter value. PSO is adjusted with random particles (models) and searches for targets by updating generations.
Herein, the PSO algorithm is applied to three synthetic data sets (residual only with and without noise, residual plus regional, residual plus anomaly generated by a buried cylinder structure) and two field gravity data sets acquired across known faults in Egypt. Assessment of the synthetic data demonstrates that the PSO algorithm generates superior results if a first horizontal gradient (FHG) filter is applied first. The robustness of the PSO inversion algorithm is demonstrated for both synthetic and field gravity data.

1. Introduction

The gravity method has an extensive variety of applications, for examples, sedimentary basin delineation (Singh and Singh, 2017), hydrocarbon exploration (Assaad, 2009; Eppelbaum and Khesin, 2012), mineral exploration (Essa, 2007; Lelièvre et al., 2012), archaeology (Linford, 2006; Panisova and Pasteka, 2009), hydrogeology (Murty and Raghavan, 2002; Al-Garni, 2005; Araffa et al., 2015), fault investigation (Essa, 2013; Abdelrahman and Essa, 2015) and cavity detection (Camacho et al., 1994; Essa, 2011). The conventional inversion of gravity data is subject to limitations including ill-poseness and non-uniqueness and requires a priori information about density contrasts (Tarantola, 2005; Essa, 2014; Mehanee, 2014; Mehanee and Essa, 2015). To over-come some of these limitations, various alternate inversion methods have been developed (e.g., Nettleton, 1962; Paul et al., 1966; Green, 1976; Jain, 1976; Telford et al., 1976; Kilty, 1983; Gupta and Pokhriyal, 1990; Abdelrahman et al., 2003; Abdelrahman et al., 2006; Abdelrahman et al., 2013; Biswas, 2015).

For example, metaheuristic techniques have been used as alternatives to the conventional inversion techniques and are designed to solve hard optimization problems with the objective of finding a more precise solution in limited time (Sen and Stoffa, 2013). These metaheuristic techniques include several different approaches including genetic algorithm (Tiampo et al., 2004; Amjadi and Naji, 2013; Kaftan, 2017), particle swarm optimization (Toushmalani, 2013; Singh and Biswas, 2016), differential evolution (Wu et al., 2014; Balkaya et al., 2017), simulated annealing (Biswas et al., 2014; Biswas et al., 2017), ant colony optimization (Liu et al., 2014; Alvandi and Asil, 2018) and hybrid genetic-price algorithm (Di Maio et al., 2016).

For the research presented herein, the particle swarm optimization (PSO) approach was used to invert gravity datasets for a 2D vertical fault structure in an effort to calculate fault parameters (depth (z), amplitude factor (K), and the origin of the fault trace (x_o)). The PSO algorithm has been applied to three synthetic data sets and two field data sets. Some of the synthetic and field Bouguer gravity data contain both residual and regional anomalies. In these cases, accuracy of the output of the PSO inversion depends on the algorithms ability to differentiate the regional and residual anomalies using the first horizontal gradient (FHG) method for several window lengths (s-value).

The PSO approach has been applied to three synthetic models. The first model represents Bouguer gravity data across a 2D vertical fault with a 1st order polynomial regional. The second model includes random noise on a pure residual gravity anomaly. The third model was designed to demonstrate the impact of an interfered structure. The PSO approach method is also applied to two real field data sets acquired

* Corresponding author.
E-mail address: mahmoudelnouishy@yahoo.com (M. Elhussein).

https://doi.org/10.1016/j.jappgeo.2020.104120
0926-9851/

across known faults in Egypt in an attempt to assess the robustness and applicability of the PSO approach when applied to real gravity data.

2. Methodology

The measured Bouguer gravity anomaly is comprised of the residual anomaly generated by the faulted structure and the undesired regional anomaly as follows:

$$\Delta g(x_i) = R(x_i, z) + Z(x_i) \quad (1)$$

where $\Delta g(x_i)$ is the Bouguer gravity anomaly (mGal), $R(x_i,z)$ is the residual gravity anomaly (mGal) and $Z(x_i)$ is the regional gravity anomaly (mGal). The objectives are to use the first horizontal gradient method to isolate the residual gravity anomaly and the PSO approach to invert it.

2.1. The 2D vertical fault forward modelling

The gravity anomaly of a 2D one-sided vertical fault or semi-infinite thin sheet can be expressed as (Abdelrahman and Essa, 2013; Hinze et al., 2013) (Fig. 1):

$$R(x_i, z) = K\left(\frac{1}{2} + \frac{1}{\pi}\tan^{-1}\left(\frac{x_i - x_o}{z}\right)\right),\ i = 1, 2, 3, 4, \ldots\ldots\ldots\ldots N \quad (2)$$

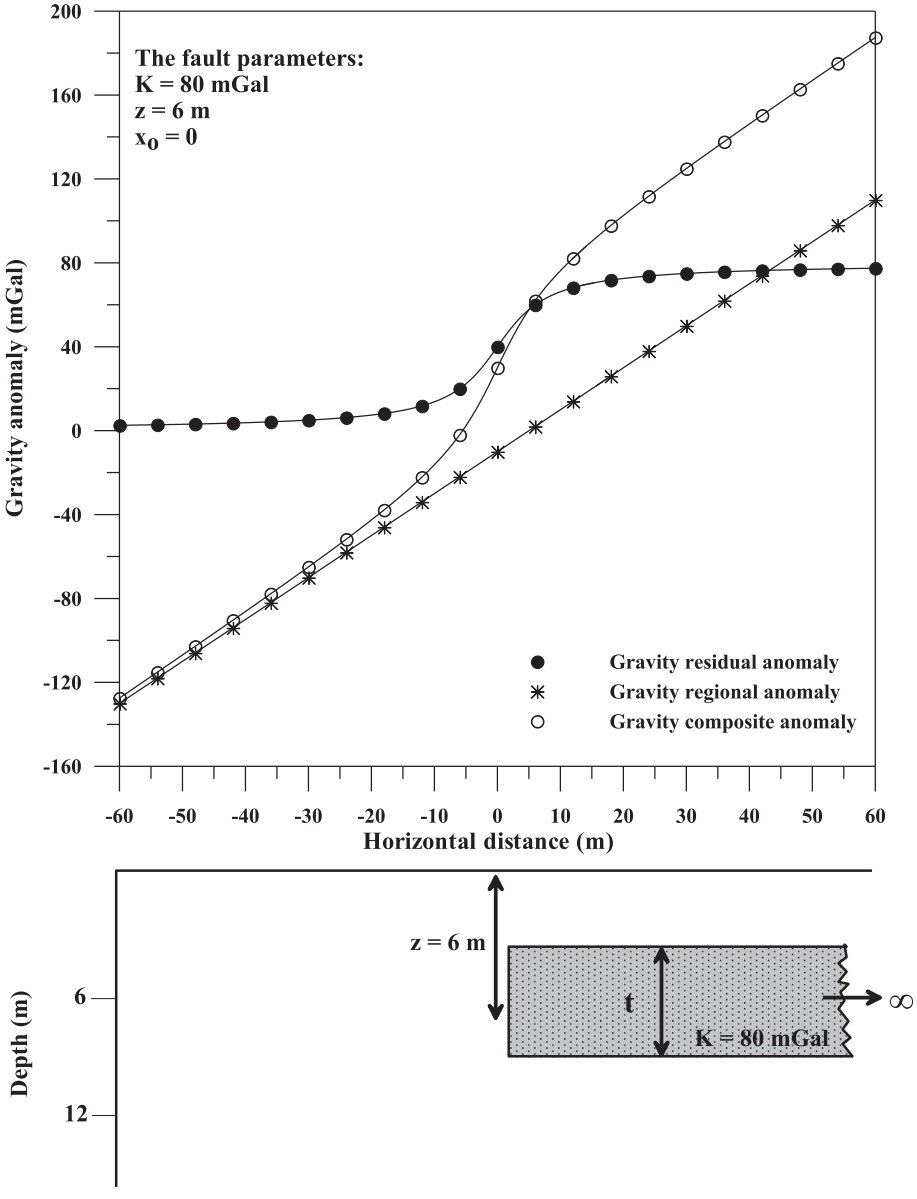

Fig. 1. Tope panel represents synthetic 2D vertical fault model (K = 80 mGal, z = 6 m, x_o = 0 m and profile length = 120 m) and a 1st-order polynomial for the regional anomaly. Lower panel represents a schematic figure showing the cross-sections and parameters.

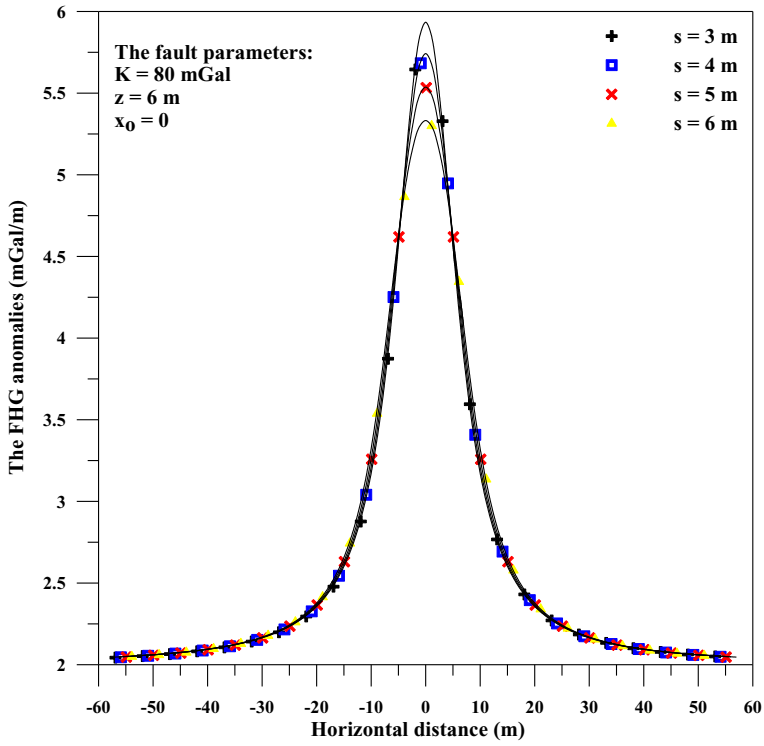

Fig. 2. FHG (first horizontal gradient) anomalies for Fig. 1.

where x_i is the horizontal location, z is the depth, x_o is the origin and K is the amplitude factor ($=2\pi G\Delta\sigma t$), G is the gravitational constant, $\Delta\sigma$ is the density contrast, and t is the thickness or throw of the fault.

2.2. The PSO inversion algorithm

The PSO algorithm was developed by Eberhart and Kennedy (1995). The PSO progression is stochastic in nature; its development was motivated by the communal in-flight performance of birds looking for food. The birds are represented by particles (or models). Individual particles have a location and a velocity vector. The location vectors represent the parameter value. PSO is adjusted with random particles (models) and searches for targets by updating generations. In each iteration, every particle updates its velocity and location using Eqs. (3) and (4) (Essa and Elhussein, 2018). The best position (T_{best}) reached by particle is kept in the memory of the particle while J_{best} model represent the best area reached by any particle. The following formulas represent the update of particle's velocity and particle's location respectively.

$$V_i^{k+1} = c_3 V_i^k + c_1 \text{rand}() \left(T_{best} - P_i^{k+1}\right) + c_2 \text{rand}() \left(J_{best} - P_i^{k+1}\right) \quad (3)$$

$$P_i^{k+1} = P_i^k + V_i^{k+1} \quad (4)$$

where v_i^k is the i^{th} particle velocity at the k^{th} iteration, $P_i^k$is the current i^{th} particle position at the k^{th} iteration, rand() is a random number between 0 and 1, c_1 and c_2 are cognitive and social coefficients and equal 2 (Parsopoulos and Vrahatis, 2002; Sweilam et al., 2007), c_3 is the inertial coefficient that governs the particle velocity and its value less than 1. The PSO algorithm was applied to several different data sets.

For those examples where a regional anomaly was present, the first horizontal gradient method was used to remove the regional background using the following approach based on Eq. (1), using two observation points ($x_i - s$, $x_i + s$) along anomaly profile. The filtered first horizontal gradient (FHG) of the gravity anomaly is assumed by the subsequent form:

$$\text{FHG}(x_i, z, s) = \frac{\Delta g(x_i + s) - \Delta g(x_i - s)}{2\,s} \quad (5)$$

where: s = 1, 2, …. M spacing units which is called graticule spacing, Δg is the Bouguer gravity anomaly.

The PSO algorithm was then applied to each FHG anomaly profile to calculate the fault parameters z, K and x_o.

For the anomalies where only residual gravity data were present, the PSO algorithm was applied directly to the Bouguer gravity data.

Table 1
Numerical results of the PSO-inversion algorithm for the Bouguer gravity anomaly profile (Fig. 1 and Eq. 8) which is consisting of a 2D vertical fault model (K = 80 mGal, z = 6 m, x_o = 0 m and profile length = 120 m) and a 1st-order polynomial for the regional gravity anomaly.

Parameters	Used ranges	Using the PSO-inversion for the Bouguer gravity data							Using the PSO-inversion for the pure residual gravity data		
		results							results	Error (%)	RMSE (mGal)
		s = 3 m	s = 4 m	s = 5 m	s = 6 m	Average-value	Error(%)	RMSE (mGal)			
K (mGal)	10–300	80	80	80	80	80 ± 0	0	0	60	25.0	76.6
z (m)	1–10	6	6	6	6	6 ± 0	0		4	33.3	
x_o (m)	−10 - 10	0	0	0	0	0 ± 0	0		−0.23	–	

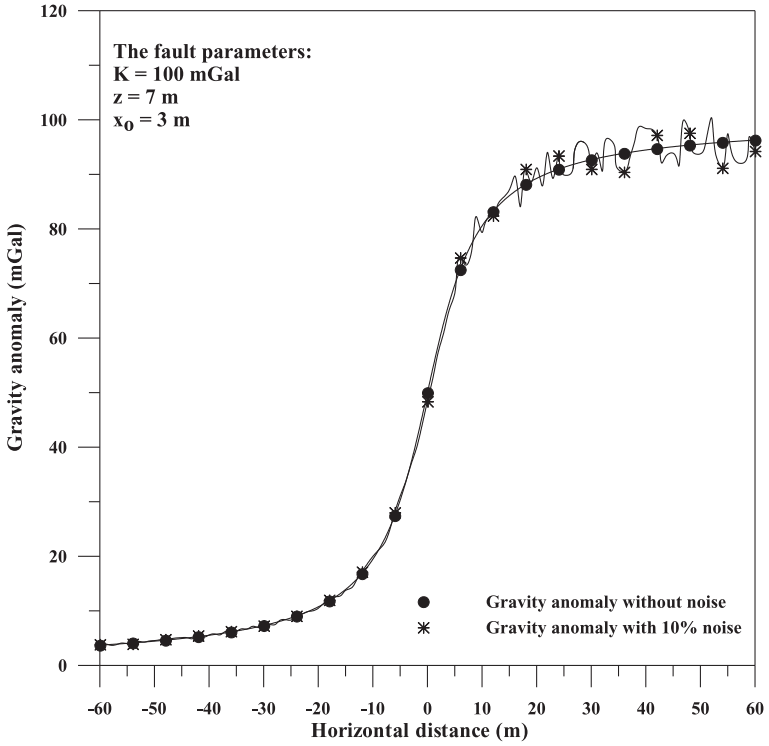

Fig. 3. Synthetic 2D vertical fault model (K = 100 mGal, z = 7 m, x_o = 3 m and profile length = 120 m) without and with a 10% random noise.

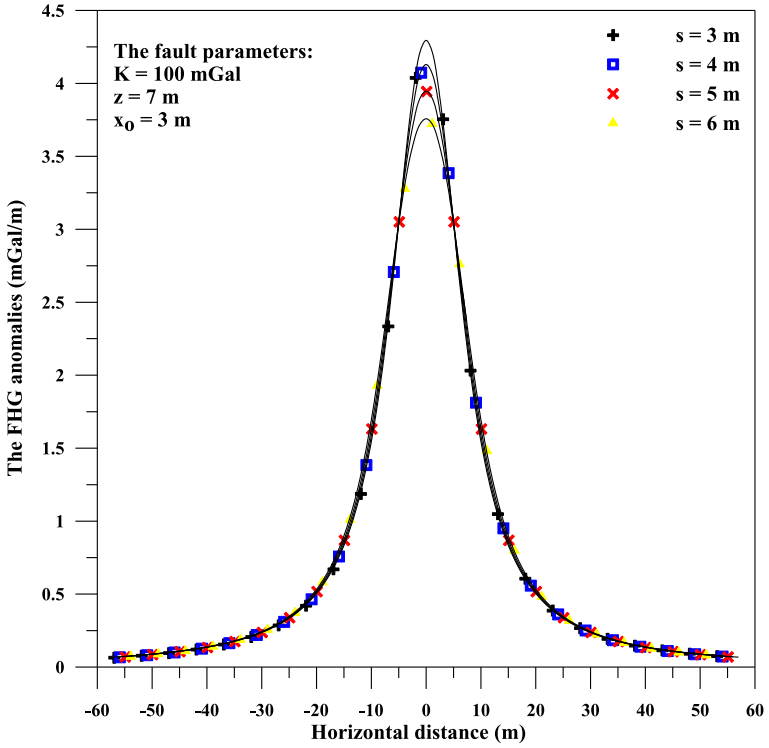

Fig. 4. FHG (first horizontal gradient) anomalies for Fig. 3 in case of 0% noise.

Table 2
Numerical results of the PSO-inversion algorithm for the residual gravity anomaly profile (Fig. 3 and Eq. 9) which is consisting of a 2D vertical fault model (K = 100 mGal, z = 7 m, x_o = 3 m and profile length = 120 m) without and with 10% random noise.

Parameters	Used ranges	Using the PSO-inversion for the Bouguer gravity data							Using the PSO-inversion for the pure residual gravity data		
		without using random noise									
		s = 3 m	s = 4 m	s = 5 m	s = 6 m	Average-value	Error (%)	RMSE (mGal)	results	Error (%)	RMSE (mGal)
K (mGal)	10–300	100	100	100	100	100 ± 0	0	0	100	0	0
z (m)	1–10	7	7	7	7	7 ± 0	0		7	0	
x_o (m)	−10 - 10	3	3	3	3	3 ± 0	0		3	0	
with using 10% random noise											
K (mGal)	10–300	116.7	111.5	108.9	90.1	106.8 ± 11.6	6.82	5.42	82.6	17.4	10.9
z (m)	1–10	6.6	7.1	6.6	7	6.83 ± 0.26	2.43		7.3	4.3	
x_o (m)	−10 - 10	2.68	2.45	2.6	2.39	2.53 ± 0.13	15.67		3.7	22.7	

2.3. The inverse modelling

Inverse modelling of gravity data across a fault is an attempt to determine the best-fit fault parameters for the Bouguer gravity data (either synthetic or real). In most cases, initial parameters must be assumed (Tarantola, 2005; Mehanee et al., 2011). A good initial model is generally developed based on available information from geology, drilling or other geophysical techniques (Zhdanov, 2002; Mehanee and Essa, 2015). The initial model is progressively refined at each iterative step until a best-fit between the measured and the predicated data is achieved. In every iterative step, the fault parameters are changed to get the best values by mimicking the next objective function (φ_{obj}), where:

$$\varphi_{obj} = \frac{2\sum_{i=1}^{N}|g_i^o - g_i^p|}{\sum_{i=1}^{N}|g_i^o - g_i^p| + \sum_{i=1}^{N}|g_i^o + g_i^p|} \quad (6)$$

N is the number of observed points, g_i^o is the observed gravity anomaly and g_i^p is the predicted gravity anomaly at the point x_i.

After estimating the fault parameters (z, K, x_o) of the 2D buried vertical fault, the whole error (RMSE) between the measured and calculated fields is estimated using the following formula:

$$\mathrm{RMSE} = \sqrt{\frac{\sum_{i=1}^{N}\left[g_i^o(x_i) - g_i^p(x_i)\right]^2}{N}} \quad (7)$$

3. Application of PSO approach to synthetic examples

The PSO inversion approach was applied to three synthetic models. The first synthetic model is the residual gravity anomaly of 2D vertical fault (K = 80 mGal, z = 6 m and x_o = 0 m) superposed on the regional field (1st order polynomial). The second model is a pure residual gravity anomaly of a 2D vertical fault (K = 100 mGal, z = 7 m and x_o = 3 m)

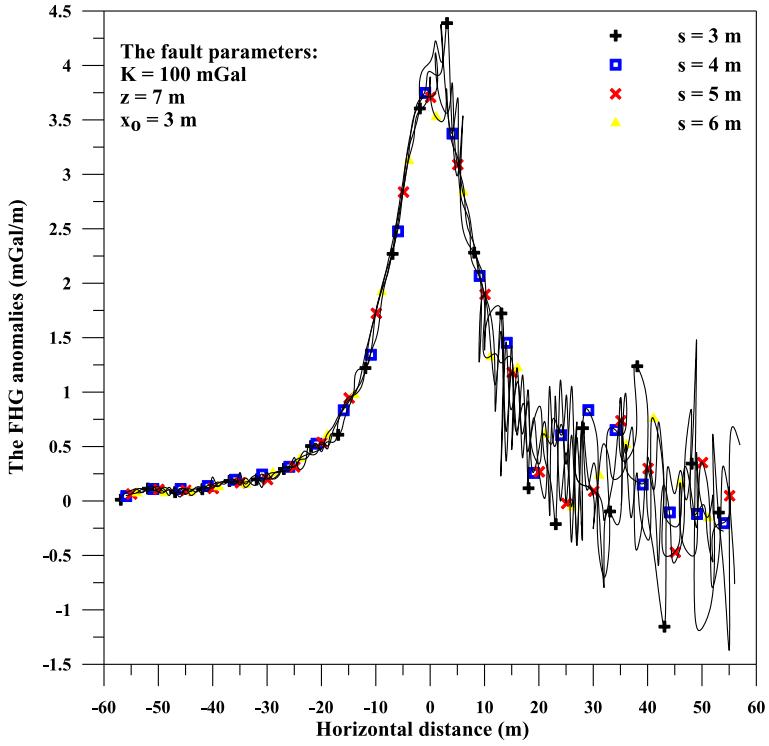

Fig. 5. FHG (first horizontal gradient) anomalies for Fig. 3 in case of 10% noise.

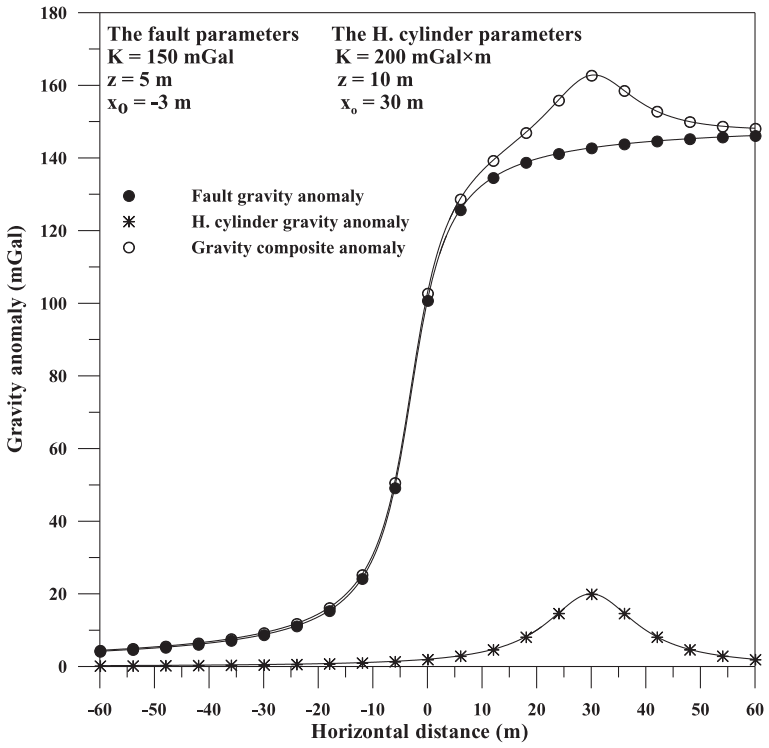

Fig. 6. Synthetic a 2D vertical fault model (K = 150 mGal, z = 5 m, x_o = −3 m and profile length = 120 m) and an interfered structure of a horizontal cylinder model (K = 200 mGal×m, z = 10 m, x_o = 30 m and profile length = 120 m).

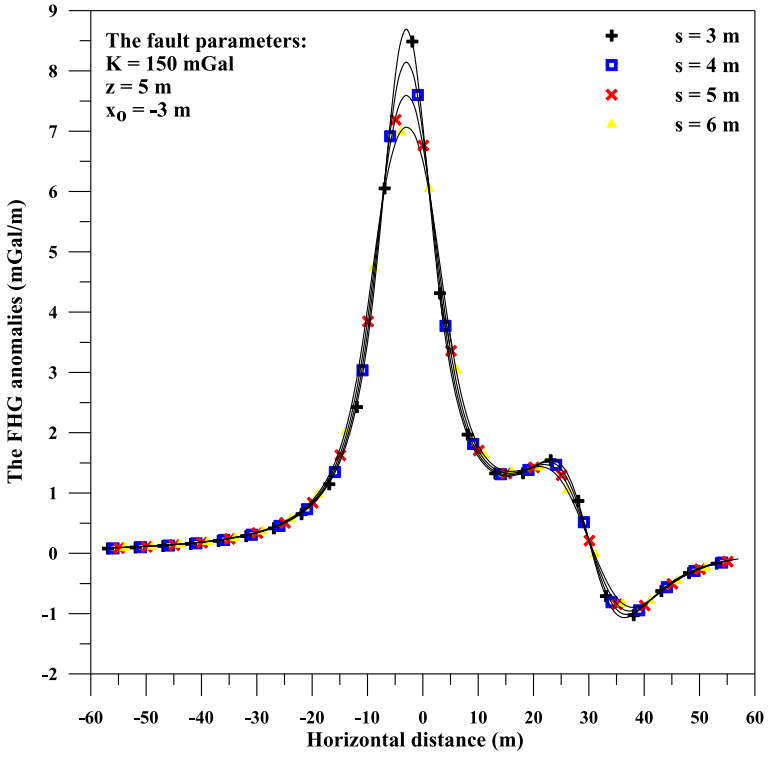

Fig. 7. FHG (first horizontal gradient) anomalies for Fig. 6.

Table 3
Numerical results of the PSO-inversion algorithm for the Bouguer gravity anomaly profile (Fig. 6 and Eq. 10) which is consisting of a 2D vertical fault model (K = 150 mGal, z = 5 m, $x_o = -3$ m and profile length = 120 m) and an interfered structure of a horizontal cylinder model (K = 200 mGal×m, z = 10 m, $x_o = 30$ m and profile length = 120 m).

Parameters	Used ranges	Using the PSO-inversion for the Bouguer gravity data							Using the PSO-inversion for the pure residual gravity data		
		results							results	Error (%)	RMSE (mGal)
		s = 3 m	s = 4 m	s = 5 m	s = 6 m	Average-value	Error (%)	RMSE (mGal)			
K (mGal)	10–300	141.4	152.88	162.28	169.88	156.6 ± 12.3	4.4	4.4	143.6	4.3	11.1
z (m)	1–10	5.1	5.1	5.2	5.2	5.2 ± 0.1	3		5.1	2	
x_o (m)	−10 − 10	−2.9	−2.9	−2.9	−2.8	−2.9 ± 0.03	3		−3.02	0.6	

without and with 10% noise. The third model is the residual anomaly of 2D vertical fault superposed on the gravity anomaly generated by a proximal buried cylindrical structure the effect of interfered structure with the target source.

3.1. 1st synthetic model

The first model consists of a 2D vertical fault with K = 80 mGal, z = 6 m, $x_o = 0$ m, profile length = 120 m plus a 1st order polynomial (regional background) (Fig. 1) as:

$$\Delta g(x_i, z) = 80\left[\frac{1}{2} + \frac{1}{\pi}\tan^{-1}\left(\frac{x_i}{6}\right)\right] + (2x_i - 10) \quad (8)$$

The FHG method was used to minimize the regional anomaly at various window lengths (s = 3, 4, 5 and 6 m) (Fig. 2). The PSO inversion algorithm was then used to calculate the fault parameters (z, K, x_o) for every s-value (Table 1). Table 1 is a summary of the assessed results and the ranges of every parameter. The assessed results for each parameter (z, K, x_o) are in close agreement with the known input model parameters.

The combination anomaly (regional and residual) was also treated as a pure residual anomaly and inverted using the PSO approach. The results are summarized in Table 1. The errors in model parameters (z, K) are 33.3% and 25%, respectively, and the RMSE is 76.6 mGal. These results indicate that the PSO inversion algorithm is not effective in the presence of a significant regional anomaly.

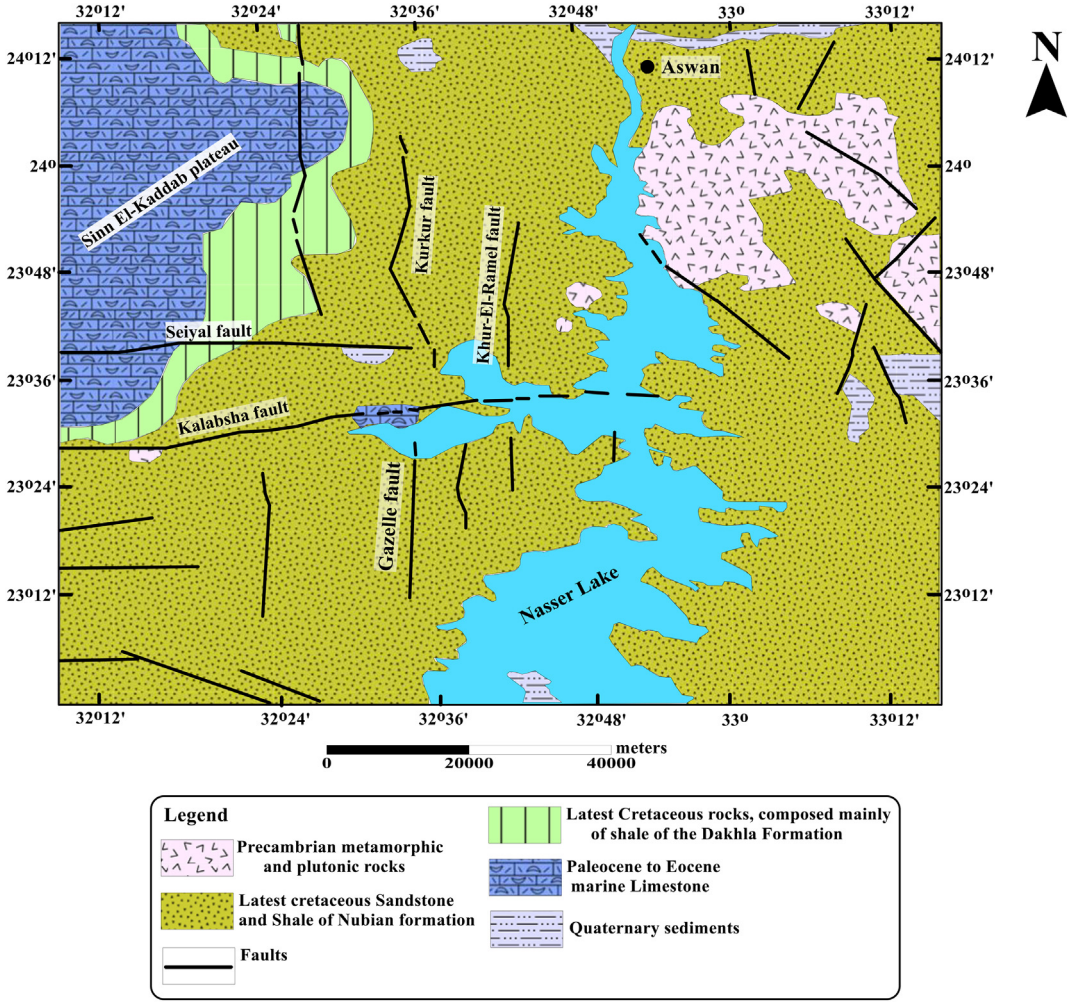

Fig. 8. Geological map of South Aswan area, showing the location of the Gazelle fault (modified after Woodward-Clyde Consultants., 1985; Abdelrahman et al., 2013).

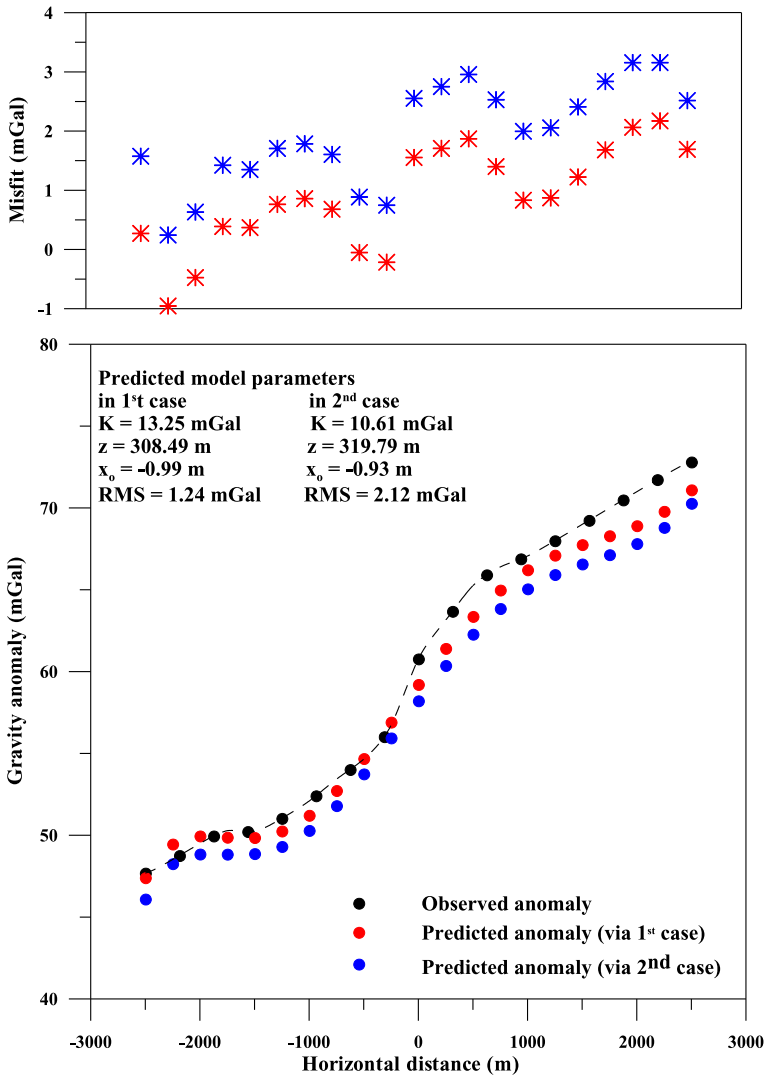

Fig. 9. Top panel represents the misfit between the observed and the predicted anomaly. Lower panel is the observed and predicted gravity anomaly for Gazelle fault, Egypt.

3.2. 2nd synthetic model

The second model consist of a pure residual gravity anomaly for a 2D vertical fault with K = 100 mGal, z = 7 m, x_o = 3 m, profile length = 120 m (Fig. 3) and can be described as:

$$\Delta g(x_i, z) = 100\left[\frac{1}{2} + \frac{1}{\pi}\tan^{-1}\left(\frac{x_i - 3}{7}\right)\right] \quad (9)$$

The FHG method was used to simulate the minimization of the non-existent regional anomaly at various window lengths (s = 3, 4, 5 and 6 m) (Fig. 4). The PSO inversion algorithm was then used to calculate the fault parameters (z, K, x_o) for every s-value (Table 2). Table 2 indicates that the output parameters are similar to the actual model parameters. The errors in all parameters and the RMSE are zero.

In order to study the effect of background noise, 10% random noise was added to the residual gravity anomaly (Eq. (9)) (Fig. 3). The process described above was used to calculate the fault parameters (z, K, x_o) for a 2D vertical fault model. The FHG anomalies are represented in Fig. 5 for the same s-value (s = 3, 4, 5 and 6 m). The estimated fault parameters are tabulated in Table 2. As noted, the PSO inversion of noisy data after the application of the FHG algorithm is superior to simply processing data without applying FHG because the RMSE = 5.42 mGal (in the 1st case) and is less than the RMSE (10.9 mGal) in the 2nd case.

3.3. 3rd synthetic model

The third model consists of a 2D vertical fault with K = 150 mGal, z = 5 m, $x_o = -3$ m, profile length = 120 m and a proximal buried horizontal cylinder with K = 200 mGal×m, z = 10 m, and x_o = 30 m (Fig. 6) described by the following formula:

$$\Delta g(x_i, z) = 150\left[\frac{1}{2} + \frac{1}{\pi}\tan^{-1}\left(\frac{x_i + 3}{5}\right)\right] + \frac{2000}{\left[(x_i - 30)^2 + 100\right]} \quad (10)$$

The FHG algorithm and PSO inversion were applied to the interfered gravity model. The FHG gravity anomalies for numerous s-values (s = 3, 4, 5 and 6 m) are depicted in Fig. 7. The output fault parameters estimated are presented in Table 3. Table 3 shows that the RMSE (4.4 mGal) for the Bouguer gravity data is less than the RMSE (11.1 mGal) for the gravity data when used directly, implying it is best to apply the FHG method first to the gravity data to remove the unwanted anomalies.

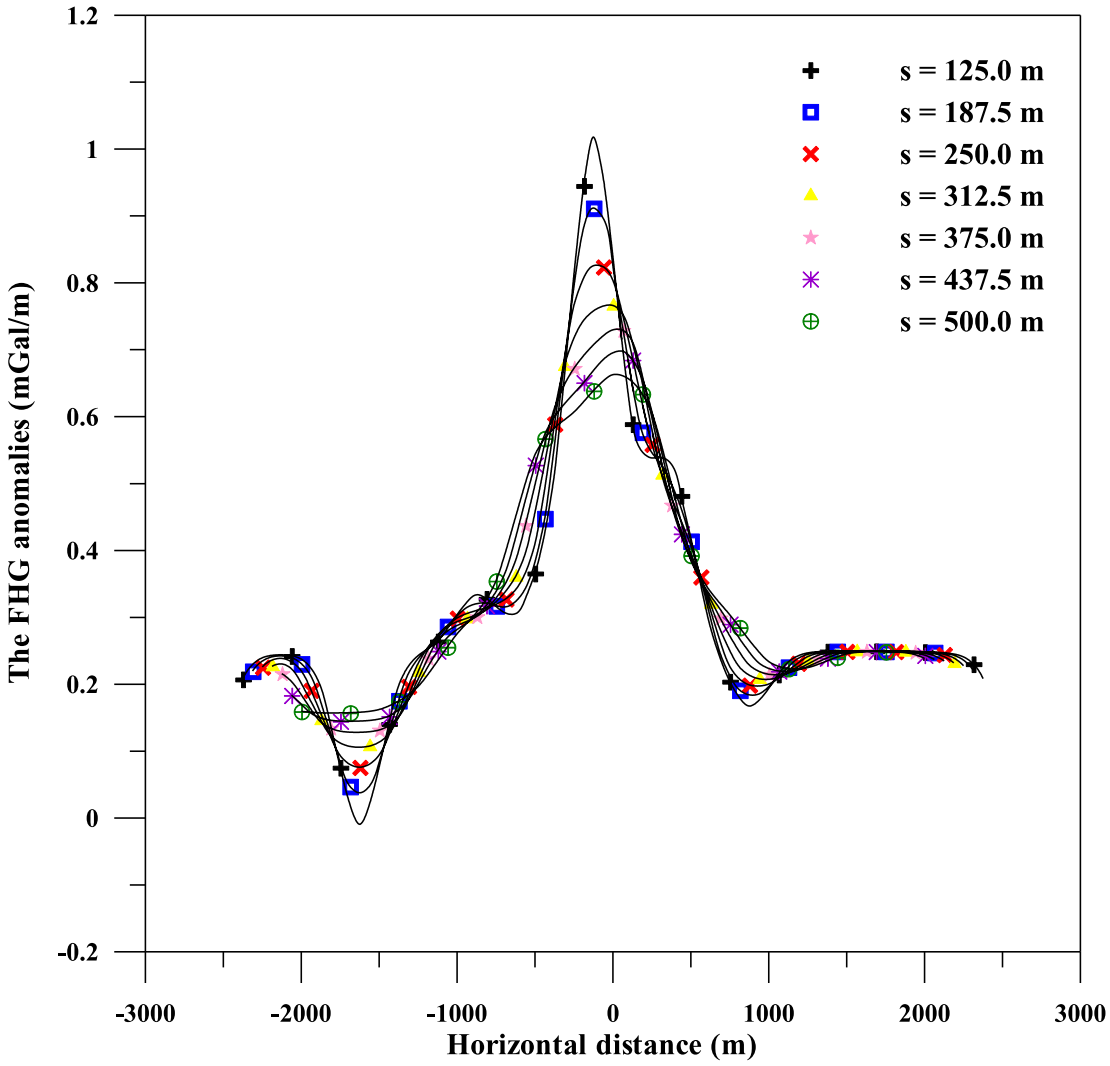

Fig. 10. FHG (first horizontal gradient) anomalies for Fig. 9.

4. Application of PSO approach to field examples

Two field examples from Egypt were inverted to demonstrate the robustness and efficiency of the PSO inversion algorithm. The importance of this study is to explore various subsurface issues related to fault or lineament analysis.

4.1. Gazelle fault example, Egypt

The Gazelle fault is located south of Aswan and trends N-S, has a length of 35 km and an inferred left-slip sense of displacement with no active features or ground cracks observed along the fault trace. The fault plane is nearly vertically (Issawi, 1969). The composite fault plane description indicates a nearly strike-slip fault with a normal-fault component (Fat-Helbary and Tealeb, 2002; Sawires et al., 2015). This fault is situated wholly through rocks latest Cretaceous sandstones and shale of Nubian Formation (Woodward-Clyde Consultants, 1985; Abdelrahman et al., 2013) (Fig. 8). Fig. 9 shows a Bouguer gravity profile of length 5000 m and was digitized at an interval of 62.5 m. First case, the PSO inversion algorithm was applied to the FHG anomalies using Eq. (5) and different s-value (s = 125, 187.5, 250, 312.5, 375, 437.5

Table 5
Numerical results for the Gazelle fault, Egypt using the second technique.

Parameters	Used ranges	Results	RMSE (mGal)
K (mGal)	1–100	10.61	2.12
z (m)	150–400	319.79	
x_o (m)	−6 - 6	−0.93	

Table 4
Numerical results for the Gazelle fault, Egypt using the first technique.

Parameters	Used ranges	Results							Average	RMSE (mGal)
		s = 125 m	s = 187.5 m	s = 250 m	s = 312.5 m	s = 375 m	s = 437.5 m	s = 500 m		
K (mGal)	1–100	16.27	11.67	13.25	9.62	14.37	11.71	15.83	13.25 ± 2.42	1.24
z (m)	150–400	321.88	309.38	300.63	269.37	314.39	318.13	325.63	308.49 ± 19.12	
x_o (m)	−6 - 6	−0.91	−1	−1	−1.04	−0.79	−0.96	−1.28	−0.99 ± 0.15	

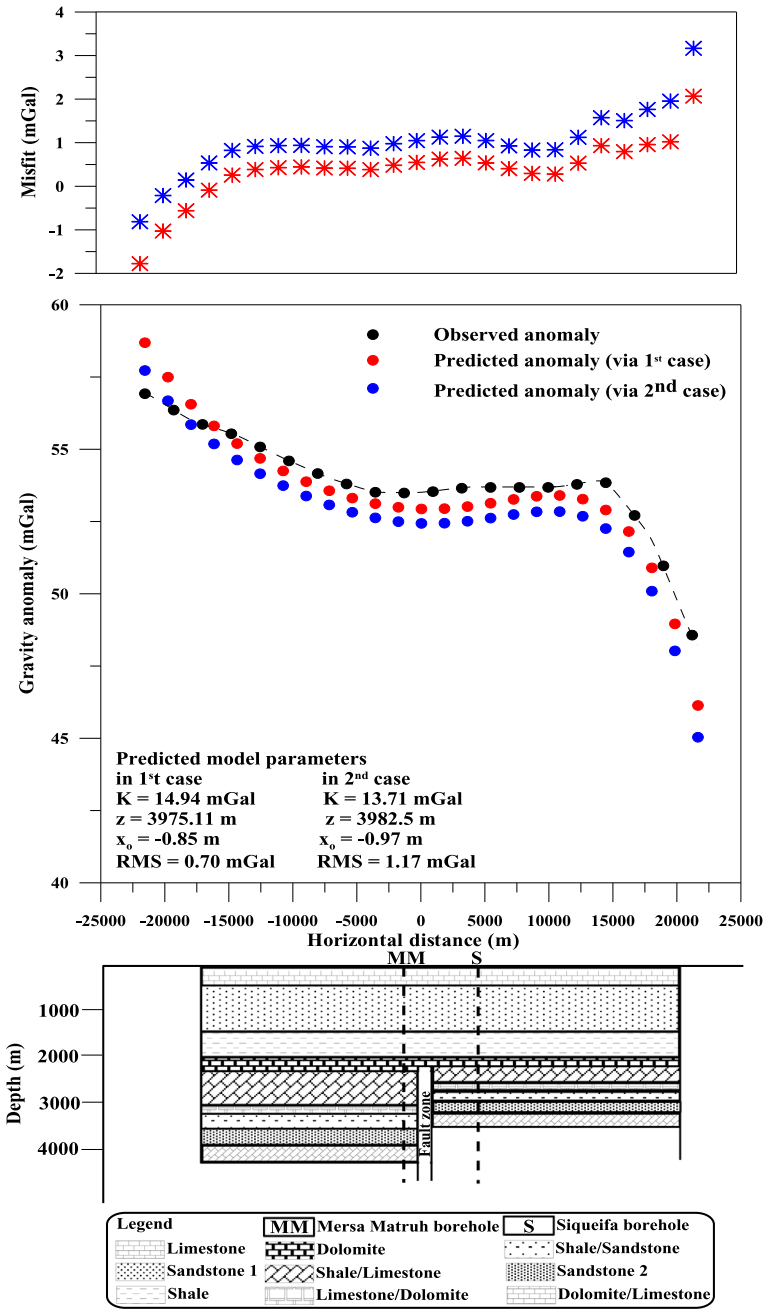

Fig. 11. Top panel represents the misfit between the observed and the predicted anomaly. Middle panel is the observed and predicted gravity anomaly for Mersa Matruh fault, Egypt. Lower panel is the geologic cross-section.

and 500 m) (Fig. 10). The estimated results are K = 13.25 ± 2.42 mGal, z = 308.49 ± 19.12 m and x_o = −0.99 ± 0.15 m with the RMSE = 1.24 mGal (Table 4). Second case, the PSO inversion algorithm was also applied to the Bouguer gravity data considering these data as the pure residual gravity anomaly. The predicated result are: K = 10.61 mGal, z = 319.79 m and x_o = −0.93 m with a RMSE = 2.12 mGal (Table 5). The results by using the PSO method convolved with the FHG method have a reasonable agreement with the results attained from drilling information (z = 300 m) (Evans et al., 1991; Abdelrahman et al., 2013; Essa, 2013; Abdelrahman and Essa, 2015).

4.2. Mersa Matruh fault example, Egypt

The Mersa Matruh fault example is from the Mersa Matruh basin in the Northwestern Desert of Egypt. The fault zone trends NE-SW as determined from stratigraphy of the boreholes MM (Mersa Matruh) and S (Siqueifa) in the study area (Fig. 11). According to Said (1962) and Barakat and Darwish (1984), the faulting is Lower Cretaceous in age. The throw of the fault is nearly 610 m and the depth extent of the fault is more than 4000 m. A Bouguer gravity anomaly profile of length 43,200 m (Fig. 11) was digitized at an interval of 450 m. First case, the digitized profile was subjected to FHG filtering using different s-value (s = 900, 1350, 1800, 2250, 2700, 3150 and 3600 m) (Fig. 12). The PSO inversion algorithm was applied to the output FHG anomalies to obtain the fault parameters (Table 6). The calculated parameters are consistent with borehole information. Second case, the PSO inversion algorithm was also applied to the Bouguer gravity data considering these data as the pure residual gravity anomaly, the predicted results were shown in Table 7.

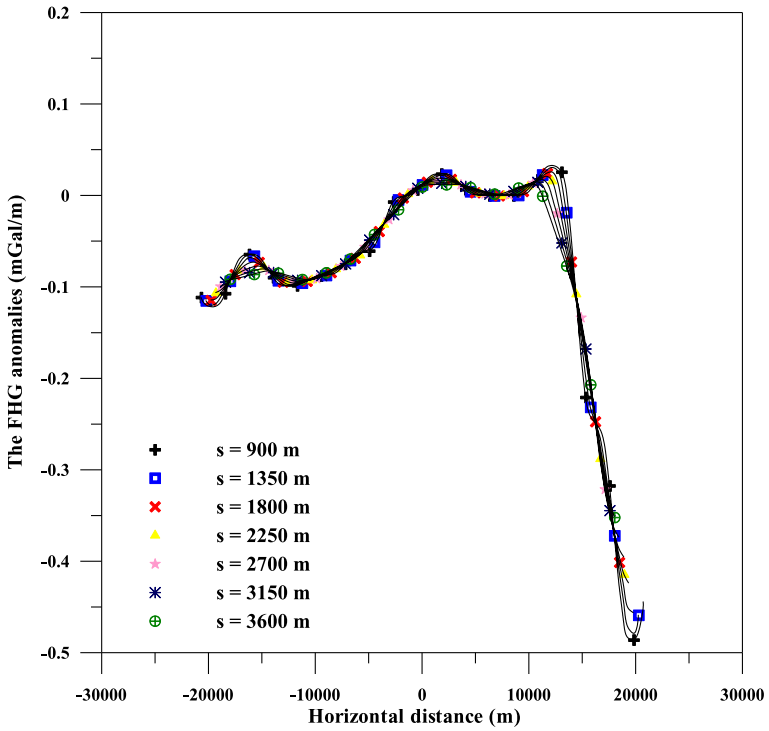

Fig. 12. FHG (first horizontal gradient) anomalies for Fig. 11.

Table 6
Numerical results for the Mersa Matruh fault, Egypt using the first technique.

Parameters	Used ranges	Results							Average	RMSE (mGal)
		s = 900 m	s = 1350 m	s = 1800 m	s = 2250 m	s = 2700 m	s = 3150 m	s = 3600 m		
K (mGal)	1–100	13.87	14.04	14.61	15.27	15.81	14.97	16.02	14.94 ± 0.83	0.70
z (m)	1500–4500	3825	3892.5	3928.5	3955.54	4009.47	4056.75	4158	3975.11 ± 110.46	
x_o (m)	−6 - 6	−0.74	−0.79	−0.83	−0.68	−0.91	−0.97	−1.04	−0.85 ± 0.13	

Table 7
Numerical results for the Mersa Matruh fault, Egypt using the second technique.

Parameters	Used ranges	Results	RMSE (mGal)
K (mGal)	1–100	13.71	1.17
z (m)	1500–4500	3982.5	
x_o (m)	−6 - 6	−0.97	

5. Conclusions

The robustness of the PSO-inversion algorithm was demonstrated for both synthetic and real gravity data and for residual gravity data (only) and residual plus regional gravity data. The gravity data processing was a two-step process. In step 1, the FHG algorithm is applied to minimize regional trends and background noise. In step 2, the PSO inversion algorithm is applied to determine fault parameters. The assessment of results confirmed that the FHG method is more stable than the conventional direct interpretation of gravity data. The PSO applications to the interpretation of the fault models is superior because it does not need a priori model information, provides for quick convergence and is robust with respect to the computation of the model parameters. In subsequent studies, this approach will be extended to the analyses of magnetic and self-potential anomalies in support of mineral exploration.

Data availability

The data will be available upon request.

Authors' contributions

Anderson N. L., Khalid S. Essa and Mahmoud Elhussein wrote the text, Anderson N. L. revised the text. Khalid S. Essa and Mahmoud Elhussein interpreted synthetic examples, Khalid S. Essa, Mahmoud Elhussein and Anderson N. L. interpreted field examples, Mahmoud Elhussein produced Figures and Khalid S. Essa produced Tables. Mahmoud Elhussein, Khalid S. Essa and Anderson N. L., made the replies to the reviewers' comments.

Declaration of Competing Interest

The authors declare that they have no known competing financial interests or personal relationships that could have appeared to influence the work reported in this paper.

Acknowledgments

The authors would like to thank Prof. Dr. Maurizio Fedi, Co-Editor-in-Chief, Prof. Dr. Afif Saad, Associate Editor, and the two reviewers for their very constructive criticisms and recommendations.

References

Abdelrahman, E.M., Essa, K.S., 2013. A new approach to semi-infinite thin slab depth determination from second moving average residual gravity anomalies. Explor. Geophys. 44, 185–191.
Abdelrahman, E.M., Essa, K.S., 2015. Three least-squares minimization approaches to interpret gravity data due to dipping faults. Pure Appl. Geophys. 172, 427–438.
Abdelrahman, E.M., El-Araby, T.M., Essa, K.S., 2003. Shape and depth solutions from third moving average residual gravity anomalies using the window curves method. Kuwait J. Sci. Eng. 30, 95–108.
Abdelrahman, E.M., Abo-Ezz, E.R., Essa, K.S., El-Araby, T.M., Soliman, K.S., 2006. A least-squares variance analysis method for shape and depth estimation from gravity data. J. Geophys. Eng. 3, 143–153.
Abdelrahman, E.M., Essa, K.S., Abo-Ezz, E.R., 2013. A least-squares window curves method to interpret gravity data due to dipping faults. J. Geophys. Eng. 10, 025003.
Al-Garni, M.A., 2005. Investigating the groundwater occurrence in Wadi Rahjan and its potential contribution to Ain Zubaida using magnetic and electric methods, Makkah Al-Mukarramah, KSA. J. King Abdulaziz Univ. Earth Sci. 18, 23–47.
Alvandi, A., Asil, R.H., 2018. A new approach for residual gravity anomalies interpretations: artificial bee colony optimization algorithm. J. Indian Geophys. Union 22, 24–31.
Amjadi, A., Naji, J., 2013. Application of genetic algorithm optimization and least square method for depth determination from residual gravity anomalies. Global J. Sci. Eng. Technol. 11, 114–123.
Araffa, S.A.S., Sabet, H.S., Gaweish, W.R., 2015. Integrated geophysical interpretation for delineating the structural elements and groundwater aquifers at central part of Sinai Peninsula Egypt. J. Afr. Earth Sci. 105, 93–106.
Assaad, F.A., 2009. Surface Geophysical Petroleum Exploration Methods. Field Methods for Petroleum Geologists. Springer, Berlin, Heidelberg.
Balkaya, C., Ekinci, Y.L., Gokturkler, G., Turan, S., 2017. 3D non-linear inversion of magnetic anomalies caused by prismatic bodies using differential evolution algorithm. J. Appl. Geophys. 136, 372–386.
Barakat, M.G., Darwish, M., 1984. Contribution to the Litho-Stratigraphy of the Lower Cretaceous Sequence in Mersa Matruh Area, North Western Desert, Egypt. Paper presented at Egyptian Petroluem Exploration Society, Cairo.
Biswas, A., 2015. Interpretation of residual gravity anomaly caused by simple shaped bodies using very fast simulated annealing global optimization. Geosci. Front. 6, 875–893.
Biswas, A., Mandal, A., Sharma, S.P., Mohanty, W.K., 2014. Delineation of subsurface structure using self-potential, gravity and resistivity surveys from South Purulia Shear Zone, India: Implication to uranium mineralization. Interpretation 2 (2), T103–T110.
Biswas, A., Parija, M.P., Kumar, S., 2017. Global nonlinear optimization for the interpretation of source parameters from total gradient of gravity and magnetic anomalies caused by thin dyke. Ann. Geophys. 60 (2), G0218.
Camacho, A.G., Vieira, R., Montesinos, F.G., Cuellar, V., 1994. A gravimetric 3D Global inversion for cavity detection. Geophys. Prospect. 42, 113–130.
Di Maio, R., Rani, P., Piegari, E., Milano, L., 2016. Self-potential data inversion through a genetic-price algorithm. Comput. Geosci. 94, 86–95.
Eberhart, R.C., Kennedy, J., 1995. A new optimizer using particle swarm theory. Proceedings of the Sixth International Symposium on micro Machine and Human Science. IEEE service center, Piscataway, NJ, Nagoya, Japan, pp. 39–43.
Eppelbaum, L.V., Khesin, B.E., 2012. Geophysical Studies in the Caucasus. Springer, p. 2012.
Essa, K.S., 2007. A simple formula for shape and depth determination from residual gravity anomalies. Acta Geophys. 55, 182–190.
Essa, K.S., 2011. A new algorithm for gravity or self-potential data interpretation. J. Geophys. Eng. 8, 434–446.
Essa, K.S., 2013. Gravity interpretation of dipping faults using the variance analysis method. J. Geophys. Eng. 10, 015003.
Essa, K.S., 2014. New fast least-squares algorithm for estimating the best-fitting parameters of some geometric-structures to measured gravity anomalies. J. Adv. Res. 5, 57–65.
Essa, K.S., Elhussein, M., 2018. PSO (Particle Swarm Optimization) for Interpretation of magnetic Anomalies caused by simple geometrical structures. Pure Appl. Geophys. 175, 3539–3553.
Evans, K., Beavan, J., Simpson, D., 1991. Estimating aquifer parameters from analysis of forced fluctuations in well level: An example from the Nubian Formation near Aswan, Egypt: 1. Hydrogeological background and large-scale permeability estimates. J. Geophys. Res. 96 (B7) 12, 127–12,137.
Fat-Helbary, R.E., Tealeb, A.A., 2002. A study of seismicity and earthquake hazard at the proposed Kalabsha Dam Site, Aswan, Egypt. Nat. Hazards 25, 117–133.
Green, R., 1976. Accurate determination of the dip angle of a geological contact using the gravity method. Geophys. Prospect. 24, 265–272.
Gupta, O.P., Pokhriyal, S.K., 1990. New formula for determining the dip angle of a fault from gravity data. SEG Tech. Progr. Exp. Abstr. 9, 646–649.
Hinze, W.J., von Frese, R.R.B., Saad, A.H., 2013. Gravity and Magnetic Exploration – Principles, Practices, and Applications. Cambridge University Press.
Issawi, B., 1969. The geology of Kurkur-Dungul Area. General Egyptian organization for geological research and mining; Cairo, Egypt. Geol. Surv. 46, 101.
Jain, S., 1976. An automatic method of direct interpretation of magnetic profiles. Geophysics 41, 531–541.
Kaftan, I., 2017. Interpretation of magnetic anomalies using a genetic algorithm. Acta Geophys. 65, 627–634.
Kilty, K.T., 1983. Werner deconvolution of profile potential field data. Geophysics 48, 234–237.
Lelièvre, P.G., Farquharson, C.G., Hurich, C.A., 2012. Joint inversion of seismic traveltimes and gravity data on unstructured grids with application to mineral exploration. Geophysics 77, K1–K15.
Linford, N., 2006. The application of geophysical methods to archaeological prospection. Rep. Prog. Phys. 69, 2205–2257.
Liu, S., Hu, X., Liu, T., 2014. A stochastic inversion method for potential field data: ant colony optimization. Pure Appl. Geophys. 171, 1531–1555.
Mehanee, S.A., 2014. Accurate and efficient regularized inversion approach for the interpretation of isolated gravity anomalies. Pure Appl. Geophys. 171, 1897–1937.
Mehanee, S.A., Essa, K.S., 2015. 2.5D regularized inversion for the interpretation of residual gravity data by a dipping thin sheet: numerical examples and case studies with an insight on sensitivity and non-uniqueness. Earth, Planets Space 67, 130.
Mehanee, S., Essa, K.S., Smith, P.D., 2011. A rapid technique for estimating the depth and width of a two-dimensional plate from self-potential data. J. Geophys. Eng. 8, 447–456.
Murty, B., Raghavan, V., 2002. The gravity method in groundwater exploration in crystalline rocks: a study in the peninsular granitic region of Hyderabad, India. Hydrogeol. J. 10, 307–321.
Nettleton, L.L., 1962. Gravity and magnetics for geologists and seismologists. AAPG Bull. 46, 1815–1838.
Panisova, J., Pasteka, R., 2009. The use of microgravity technique in archaeology: a case study from the St. Nicolas Church in Pukanec, Slovakia. Contrib. Geophys. Geodesy 39, 237–254.
Parsopoulos, K.E., Vrahatis, M.N., 2002. Recent approaches to global optimization problems through particle swarm optimization. Nat. Comput. 1, 235–306.
Paul, M.K., Datta, S., Banerjee, B., 1966. Direct interpretation of two dimensional structural fault from gravity data. Geophysics 31, 940–948.
Said, R., 1962. The Geology of Egypt. Elsevier Publishing Co.
Sawires, R., Peláez, J.A., Fat-Helbary, R.E., Ibrahim, H.A., García Hernández, M.T., 2015. An updated seismic source model for Egypt. In: Moustafa, A. (Ed.), Earthquake Engineering - From Engineering Seismology to Optimal Seismic Design of Engineering Structures. IntechOpen, London. https://doi.org/10.5772/58971.
Sen, M.K., Stoffa, P.L., 2013. Global Optimization Methods in Geophysical Inversion. Cambridge University Press, p. 302.
Singh, A., Biswas, A., 2016. Application of global particle swarm optimization for inversion of residual gravity anomalies over geological bodies with idealized geometries. Nat. Resour. Res. 25 (3), 297–314.
Singh, K.K., Singh, U.K., 2017. Application of particle swarm optimization for gravity inversion of 2.5-D sedimentary basins using variable density contrast. Geosci. Instrument. Methods Data Syst. 6, 193–198.
Sweilam, N.H., El-Metwally, K., Abdelazeem, M., 2007. Self potential signal inversion to simple polarized bodies using the particle swarm optimization method: a visibility study. J. Appl. Geophys. 6, 195–208.
Tarantola, A., 2005. Inverse Problem Theory and Methods for Model Parameter Estimation. Society for Industrial and Applied Mathematics (SIAM), Philadelphia.
Telford, W.M., Geldart, L.P., Sheriff, R.E., Keys, D.A., 1976. Applied Geophysics. Cambridge University Press.
Tiampo, K.F., Fernandez, J., Jentzschc, G., Charco, M., Rundle, J.B., 2004. Volcanic source inversion using a genetic algorithm and an elastic gravitational layered earth model for magmatic intrusions. Comput. Geosci. 30, 985–1001.
Toushmalani, R., 2013. Comparison result of inversion of gravity data of a fault by particle swarm optimization and Levenberg-Marquardt methods. SpringerPlus 2, 462.
Woodward-Clyde Consultants, 1985. Identification of earthquake sources and estimation of magnitudes and recurrence intervals. Internal Report 135, High and Aswan Dams Authority, Aswan, Egypt.
Wu, G.J., Liu, H., Zou, Z.B., Yang, G.L., Shen, C.Y., 2014. 3-Dimensional Inversion for Gravity Anomaly Calculation in complex Geologic Region. Adv. Mater. Res. 962–965, 238–241.
Zhdanov, M.S., 2002. Geophysical Inversion Theory and Regularization Problems. Elsevier, Amsterdam, p. 633.